Hindawi
Advances in Civil Engineering
Volume 2019, Article ID 4172103, 19 pages
https://doi.org/10.1155/2019/4172103

Research Article

Optimization for U-Shaped Steel Support in Deep Tunnels under Coupled Static-Dynamic Loading

Yujun Zuo,[1] **Jian Wang**,[1] **Longjun Dong**,[2] **Weiwei Shu**,[2] **Meilu Yu**,[1] **Wenjibin Sun**,[1] **and Zhonghu Wu**[3]

[1]*Mining College, Guizhou University, Guiyang 550025, China*
[2]*School of Resources and Safety Engineering, Central South University, Changsha 410083, China*
[3]*College of Civil Engineering, Guizhou University, Guiyang 550025, China*

Correspondence should be addressed to Longjun Dong; lj.dong@csu.edu.cn

Received 4 May 2018; Revised 3 July 2018; Accepted 15 January 2019; Published 21 February 2019

Academic Editor: Emilio García-Taengua

With the effects of high geostress and intensive dynamic disturbances in deep mining, the stability and safety of tunnels are seriously affected. The optimization for U-shaped steel support is of vital significance and can solve the problems of cost reduction and tunnel instability. Based on the perturbation equation, a coupled formula for U-shaped steel and the surrounding rock mass was proposed to evaluate the practical stability of a U-shaped steel support. Through a numerical simulation method, the characteristics of U-shaped steel support can be obtained under coupled static-dynamic loading. Furthermore, the field test was carried out and compared with the numerical simulation, which was discussed. The results show that there will be a stress concentration when the contact area is small. In addition, the concentrated stress will release with the increase in contact area. With the increase in the lateral stress coefficient, the deformation exhibits a downward trend under static loading, indicating that the lateral stress is the dominant force driving the deep geostress activity. The support requirement of this section of surrounding rock can be satisfied by a U-shaped steel group with 1.5 m spacing under dynamic disturbance.

1. Introduction

Due to the severe situation in the mining market in recent years, all mining enterprises are further reducing the cost and increasing efficiency, and the cost of tunnel support accounts for a large proportion of the cost of mine production materials. If the support forms and parameters of the tunnel are not chosen properly, it will cause two extremes: one is the high intensity of support, which will cause high support costs and affect the speed of excavation. The other is that the strength of support is not enough to effectively control the deformation of surrounding rock, and safety accidents can easily occur such as roof fall. How to reduce the support cost under safe conditions has become a new topic in the production of enterprises.

Because the mine production condition is special, safe, and stable, production can enter the track of the virtuous circle. Particularly, roof collapse is one of the most destructive safety accidents occurring during and after the deep tunnel excavation. According to statistical data, approximately 1200 deaths have been caused by tunnel instability in 2008 in China; tunnel instability is an accident that is difficult to predict, creates a great safety hazard, and produces strong destructiveness [1]. Therefore, to reduce the support cost, first of all, we should do a good job of safety, to solve the problem of roadway instability.

To solve the tunnel instability problem, the microseismic monitoring technology is employed to locate cracks and characterize the stress conditions for the physical processes related to rock deformation and failure, which can provide guidance for the evaluation of tunnel stability [2–5]. However, the difficulties in accurate identification and localization for microseismic sources may delay the stability

analysis; thus, tunnel safety cannot be effectively ensured. Dong et al. [6, 7] established an interval nonprobabilistic reliability model to analyze the stability of jointed rock mass. In addition, Li et al. [8–11] were the first to study the mechanical properties of rock under dynamic and static combined loading and put forward the corresponding constitutive model, as well as the two coupling loading methods "critical static stress slight disturbance" and "elastic static stress shock disturbance," and applied them to the experiment. Through the small-scale model tests, Kirsch [12] researched the evolution of failure mechanism for different overburden layers over the tunnel. Yang et al. [13] established a numerical model of tunnel ventilation using UDEC, and then the tunnel failure process was simulated. Based on the numerical simulation and laboratory experiment, Wang et al. [14] investigated the deformation characteristics, stress distribution, and stability of surrounding rock in tunnels, which provided useful information for the tunnel collapse process. However, it is worth noting that the above-mentioned research mainly focuses on the analysis of failure mechanism and process, which is a type of post hoc analysis for the excavated tunnels. Actually, it is also important to select suitable and effective supporting methods for tunnels, which can basically prevent the deep tunnel instability in a direct way, and the purpose of reducing the support cost is achieved.

Currently, the commonly used supporting technologies include shotcrete [15], bolts [16], and steel I-beams [17], and their characteristics and performances have been comprehensively discussed. Zhou et al. [18] calculated the critical buckling stress of the I-steel concrete composite beams, which provided a theoretical basis for improving the support effect of the I-steel concrete composite beams. Cao et al. [19] put forward a bolt support method for tunnels that can reduce surrounding rock deformation through optimization of bolt parameters and arrangement, floor beam layout, and full-length grouting. Although these technologies have the advantages of low support costs and improved support effects, most of them have the disadvantages including the low support strength, anti-bending capacity, and difficult applicability, which are also prominent [20, 21]. Thus, it is more suitable for them to be applied in shallow tunnels, instead of deep tunnels with high geostress. In recent years, more attention has been paid to the yieldable U-shaped steel due to its superior characteristics shown in deep tunnels, which can effectively control the surrounding rock deformation through the adaptation of proper support intensity. Liu et al. [22] explored the mechanical mechanism of U-shaped steel supports using ANSYS software. Jiao et al. [23] improved the support effects of the traditional U-shaped steel sets in a loose thick coal seam, which can accelerate the excavation and reduce cost. However, the factors including support spacing, side stress coefficient, dynamic disturbances, and contact area between U-shaped steel and surrounding rock are not comprehensively considered in the previous research, actually. The support spacing and contact area are related to tunnel stability and mine cost. In deep tunnels, horizontal stress is one of the important factors related to tunnel instability, and mine operation is affected by blasting impacts and other events. Therefore, it is significant to study the U-shaped steel support in deep tunnels under the effects of various influencing factors.

In view of this, we put forward a coupled formula for the U-shaped steel and surrounding rock in deep three-center arch tunnels that can be used to evaluate U-shaped steel failure. Then, a 3D coupled model was established using ANSYS software. With the considerations of different support spacings, side stress coefficients, contact area ratios, and dynamic disturbances, the stability of surrounding rock and the support effect of U-shaped steel were comprehensively researched. Furthermore, combined with the field blasting vibration tests, the numerical simulation results were analyzed and verified. Finally, the optimal support spacing of U-shaped steel was solved with the combination of stress concentration factor. This paper is expected to provide theoretical guidance for the U-shaped steel support of deep tunnels, which can improve tunnel stability and reduce support cost.

2. Establishment of the Coupling Model

In general, the micromodels are established to explore the mechanisms between surrounding rock and support system [24, 25], which are commonly established for the circular tunnels. On this basis, a coupling model between surrounding rock and U-shaped steel in the three-core arch tunnel is proposed. The U-shaped steel is simplified and can be regarded as a bar member, as shown in Figure 1.

2.1. Perturbation Equation Addition. The arch form exists in both U-shaped steel and surrounding rock. It is advisable that the arch deformation mode should be set as $\sin(\pi x/t)$, according to reference [25]. Combined with the static pressure and harmonic roof plate disturbance, the sum of uniform load and roof plate disturbance can be calculated as

$$Q(x,t) = F(\cos \Omega t) \cdot \sin\left(\frac{\pi x}{L}\right) + q(x,t), \tag{1}$$

where $Q(x,t)$ is the sum of uniform load and roof plate disturbance, F is the vibration amplitude, Ω is the vibration angular frequency, and $q(x,t)$ is the uniform load on the U-shaped steel roof plate.

2.2. Analysis of Coupling Failure between U-Shaped Steel and Surrounding Rock. The main form of bar failure is tensile failure. The maximum tensile stress can be calculated with the critical tensile force of the bar:

$$\sigma_{\max} = \frac{\rho L^2}{2h} - \sigma_{\mathrm{h}} = \frac{\rho L^2}{2h} - \xi \cdot Q(x,t), \tag{2}$$

where ρ is the rock mass density, ξ is the side stress coefficient, and $\sigma_{\max}$ is the maximum tensile stress.

The critical force for the pressed beam is calculated as follows:

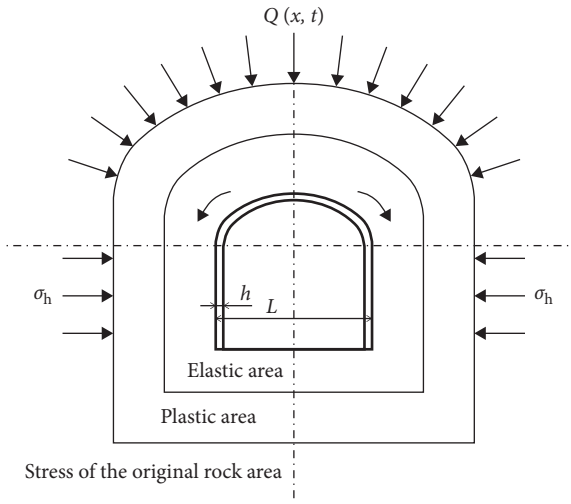

Figure 1: Coupling model of the roof of the surrounding rock and supporting body. $Q(x,t)$ is the sum of the uniform load and vibration of the roof plate, acting on the upper part of the bar; σ_h is the horizontal stress, acting on the horizontal direction of the bar; L is the length of the bar and can be the span of U-shaped steel; h is the thickness and can be set to unit length "1."

$$F_{cr} = \frac{\pi^2 EI}{(\mu L)^2} = \sigma_{cr} \cdot bh,$$
$$\sigma_{cr} = \frac{\pi^2 Eh^2}{3L^2}, \tag{3}$$

where σ_{cr} is the critical stress for the pressed beam; b is the beam width and can be set as unit length "1"; μ is the length coefficient, taken as 0.5; and I is the second moment of area.

When the maximum compressive stress of the bar is greater than the critical stress ($\sigma_{cr} < \sigma_h$), U-shaped steel will be unstable. The safety factor A determines the stability:

$$A = \frac{\sigma_{max}}{\sigma_{cr}} = \frac{[(\rho L^2/2h) - \xi \cdot Q(x,t)]}{(\pi^2 Eh^2/3L^2)} = \frac{3L^2[\rho L^2 - 2h\xi \cdot Q(x,t)]}{2\pi^2 Eh^3}. \tag{4}$$

If $A > 1$, U-shaped steel will be unstable.

If $A < 1$, U-shaped steel will be stable.

The different values of the sum of uniform load and roof plate disturbance are substituted into equation (4), and the failure curve of U-shaped steel is drawn, as shown in Figure 2. A critical point of U-shaped steel failure is obtained roughly, which is located between $E = 24$ MPa and 26 MPa, which provides some guidance for subsequent numerical simulation.

2.3. Formula Demonstration. Hypothetical surrounding rock mechanical parameters are $\sigma_c = 20$ MPa, $C = 6$ MPa, $\varphi = 25^\circ$, $G = 5$ GPa, $R_0 = 3$ m, $P_0 = 15$ MPa (low ground stress field), and $P_0 = 35$ MPa (high ground stress field).

To verify the correctness and the effectiveness of the solved formula, several groups of simulations and field related data are listed in Table 1, in which P_0 represents different vertical stresses. The stress varies when the

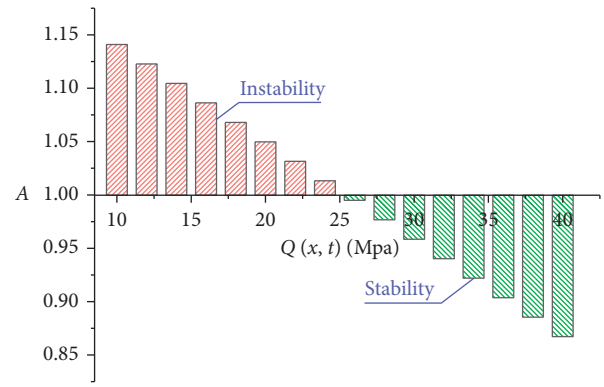

Figure 2: U-shaped steel failure curve. $Q(x,t)$ is the sum of uniform load and roof plate disturbance, and A is the factor of safety. The value of A decreases with the increase in elastic modulus $Q(x,t)$.

U-shaped steel spacing is different. The A value in all cases in the table is less than 0, which means the U-shaped steel does not break. Considering the physical parameters of surrounding rock, it is normal to meet the requirements of stability.

3. ANSYS Numerical Simulation Analysis

In order to study the support effect of U-shaped steel on-site, a coupling model between U-shaped steel and surrounding rock was established based on mine geological data. The parameters of 25 U-shaped steels and rock masses are shown in Tables 2 and 3.

In the process of numerical simulation, it is impossible to take all factors that affect the tunnel stability into account. Therefore, the simulation makes some necessary assumptions: (1) the rock mass is regarded as a continuous, homogeneous, and isotropic medium; (2) the contact surface of U-shaped steel and rock mass is in good condition with no relative slip; and (3) the effects of groundwater are not considered.

According to the degree of rock fracture in deep mines, Dong and Zhao [26] divide the quality of surrounding rock into five grades. The selected parameters are similar to those of grade II rock mass with small collapses and low strength of rock fracture section. In order to ensure the safety and stability of the tunnel, the tunnel adopts the U-shaped steel support.

The parameters in Tables 2 and 3 are inputted into the model, and 24 monitoring points are arranged on the U-shaped steel beam on average; the boundary conditions of the model are carried out, as shown in Figure 3.

3.1. Spacing Influence Factor. The rationality of U-shaped steel spacing is one of the important problems related to the redundancy of support and the economic benefit of the whole mine. More importantly, it can protect the supports from out-of-plane instability. For this purpose, the equivalent stress and deformation of U-shaped steel at different spacings were simulated, as shown in Figure 4. Among them,

Table 1: The safety factor of the coupling model between the surrounding rock and U-shaped steel.

Plan	P_0 (MPa)	K	P	Ω (Hz)	v (m/s)	t (s)	A
A	15	0.8	1/4	10	1	4.5	<0
B	20	1.0	1/3	30	2	4.6	<0
C	25	1.2	1/2	50	3	4.7	<0
D	30	1.5	3/4	70	4	4.8	<0
E	35	2.0	1	90	5	4.9	<0

K is the side stress coefficient, and P is the contact area ratio.

Table 2: The chemical composition, geometric parameters, and mechanical properties of U-shaped steel.

Chemical composition	C	Si	Mn		AL_t	P	S
	0.21~0.31	0.2~0.6	1.20~1.60		≥0.015	≤0.045	≤0.045
Geometric parameters	Sectional area (cm^2)	Weight ($kg \cdot m^{-1}$)	Moment of inertia (cm^4)		Inertial radius (cm)	Sectional modulus (cm^3)	Static moment (cm)
			I_X	I_Y	I_x I_y	W_X W_Y	S_x
	31.79	24.95	495.8	551.9	3.95 4.17	83.1 81.77	197.5
Mechanical properties	Tensile strength (MPa)	Yield strength (MPa)	Elongation at break (%)	Bending test (D = diameter (mm); A = sample thickness (mm))		Shear strength (MPa)	Young's modulus (GPa)	Poisson's ratio
	530	335	20	$D = 3A$		318	206	0.3

Table 3: Rock mechanical parameters.

Parameter	Supporting section surrounding rock
Young's modulus (GPa)	98
Poisson's ratio	0.22
Compressive strength (MPa)	75
Tensile strength (MPa)	10
Internal friction angle	35
Cohesion (MPa)	27

the distance is between 1.0 m and 2.5 m, the deformation of each monitoring point is increased, but the amount of deformation at 0.5 m is relatively large. The local single data and the overall data deviation need to be quantified.

3.2. Impact Factor of Lateral Stress Coefficient. The side stress coefficient is the ratio of vertical stress to horizontal stress, which is an important aspect of tunnel stability. The lateral stress coefficient is related to tunnel stability, so a tunnel support model with different lateral pressure coefficients and 1.5-meter spacing is established, as shown in Figure 5. It can be seen that, with the increase in lateral stress coefficient, the main force of U-shaped steel is transferred from the top beam to the side beam.

Second, the deformation values of U-shaped steel monitoring points under each side stress coefficient are extracted, and the curves are drawn, as shown in Figure 6. The black broken line deformation is the largest and the green broken line deformation is the smallest, indicating that the main force of failure and instability of deep U-shaped steel is horizontal stress.

Considering only one factor is not enough to obtain the support law, different spacings are added on the basis of different lateral stress coefficients. As shown in Figures 7(a)–7(c), it can be seen that the deformation amount of the black broken line with the distance of 0.5 m is larger than that of the 1.0 m red broken line. The deformation of the black broken line with 0.5 m spacing is smaller than that of the 1.0 m red broken line, which indicates that, with the increase in the side stress coefficient, the deformation characteristics of the U-shaped steel with small spacing will change. The side stress coefficient increased, and the outburst deformation part of U-shaped steel was transferred from the top beam to the side beam.

3.3. Impact Factor of Contact Area Ratio. In practical applications, due to construction problems, the tunnel surface is often not regular, and the erection of U-shaped steel cannot be completely aligned with the surrounding rock. Because the fitting is incomplete, the local stress concentration phenomenon often appears [27]. Stress concentration refers to the phenomenon that the maximum stress value is higher than the average stress value in the local region of the structure or member. Therefore, it is necessary to analyze the contact area ratio between U-shaped steel and surrounding rock. For this reason, a tunnel support model with a lateral pressure coefficient of 1 and a distance of 1.5 m is established, under different contact area ratios, as shown in Figure 8. From Figures 8(a)–8(c), it is found that the bottom of the U-shaped steel has less contact with the rock mass, and the equivalent stress value is higher. It can be seen from Figures 8(d)–8(f) that the equivalent stress values are smaller than those shown in Figures 8(a)–8(c). The side beam contact is relatively higher, and the equivalent stress value is low. It indicates that, with the increase in ground stress, the dangerous point of the material is the point with higher equivalent stress.

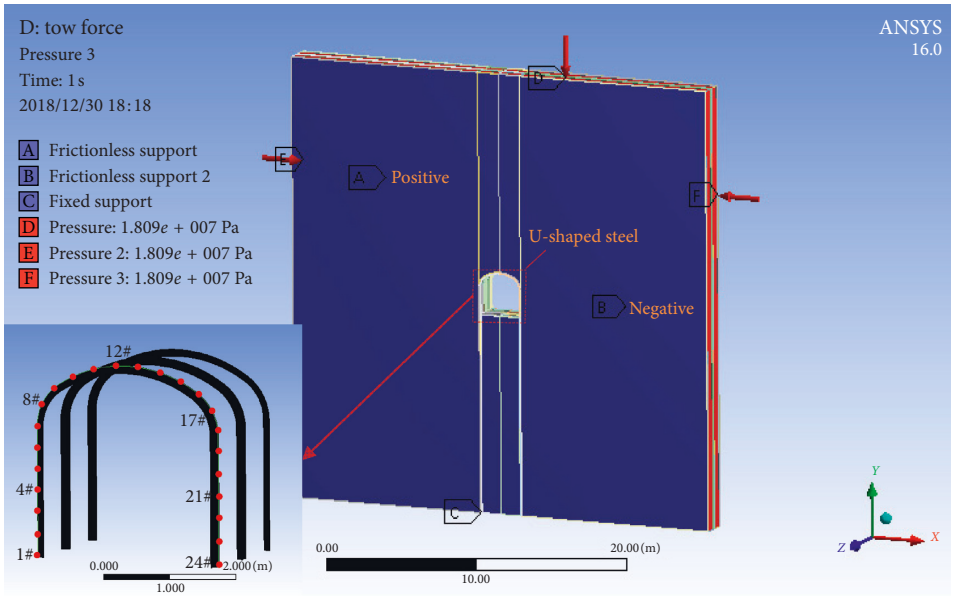

Figure 3: Coupling model of U-shaped steel and surrounding rock. The boundary conditions and 24 monitoring points are represented with A to F and red spheres.

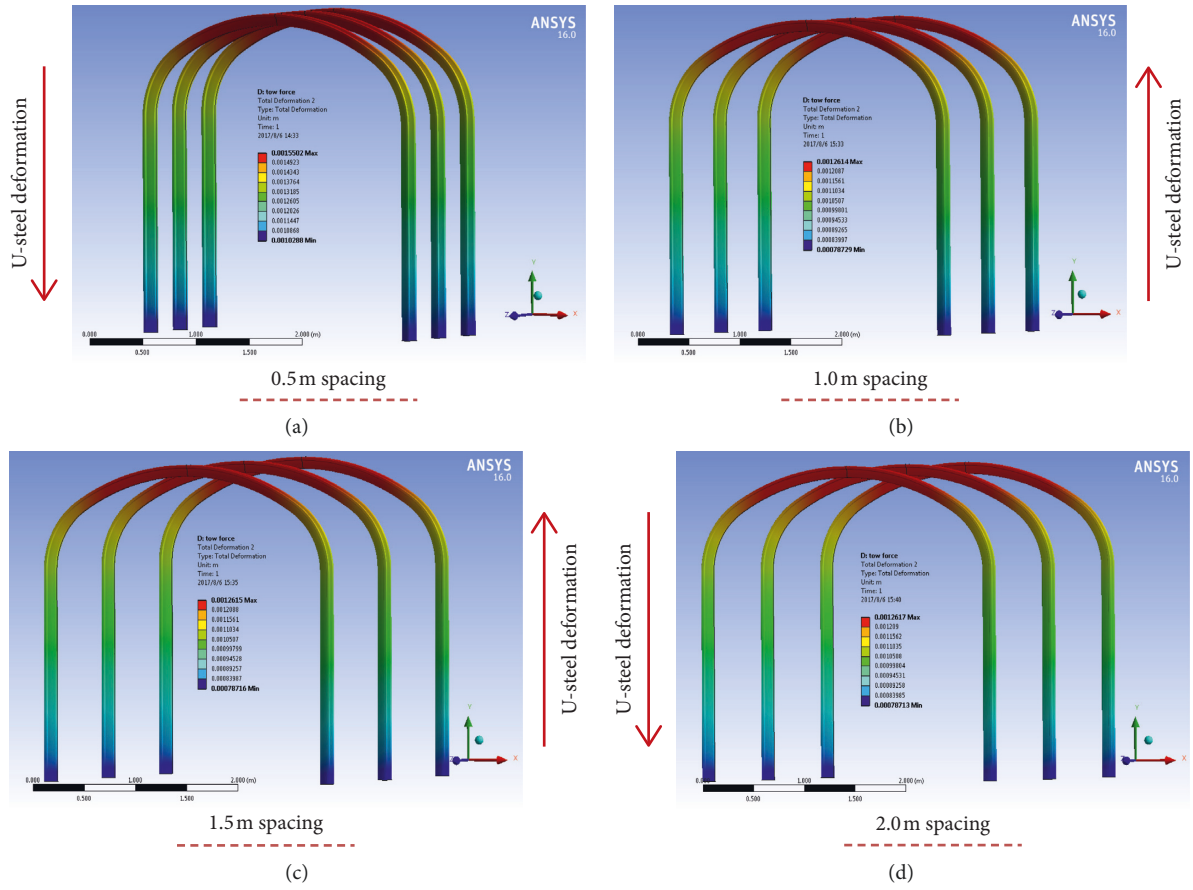

Figure 4: Continued.

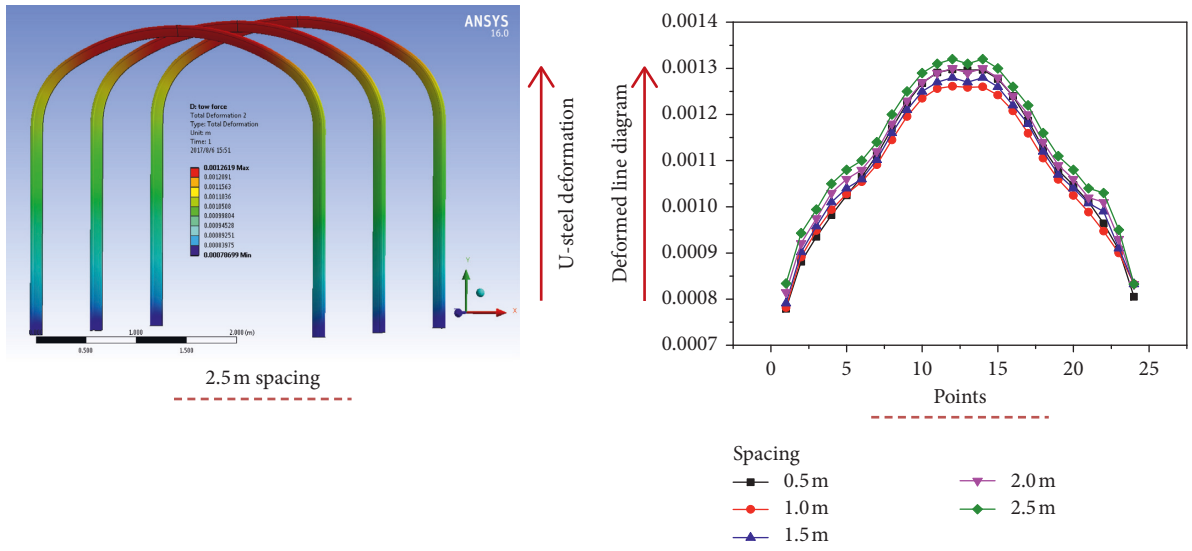

(e) (f)

Figure 4: Deformation of the U-shaped steel with different spacings: (a) 0.5 m; (b) 1.0 m; (c) 1.5 m; (d) 2.0 m; (e) 2.5 m. They are represented by the curves in black, red, blue, pink, and green, respectively. Blue to red, small to large deformation. The data from the monitoring points are extracted and drawn as the broken line map (f). The maximum values were 1.5502 mm, 1.2614 mm, 1.2615 mm, 1.2617 mm, and 1.2619 mm, respectively.

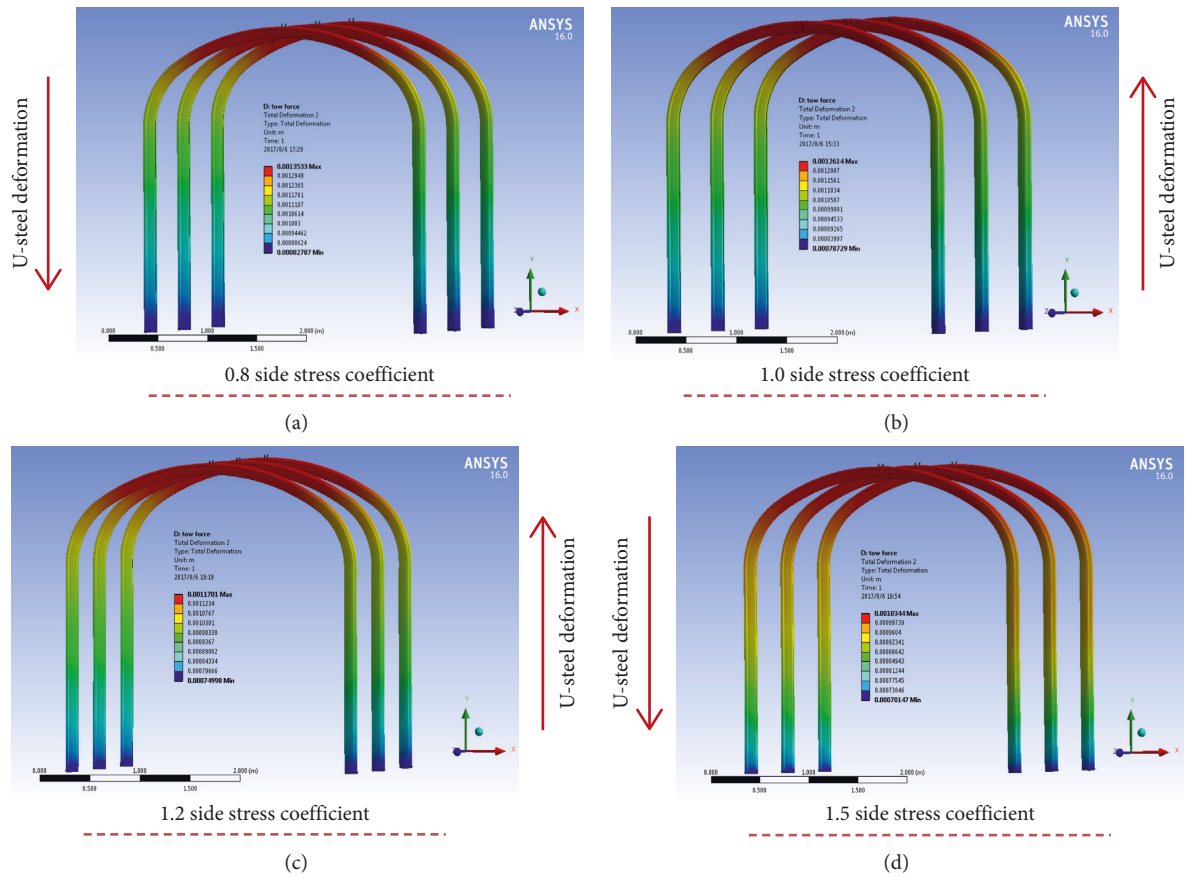

(a) (b)

(c) (d)

Figure 5: Continued.

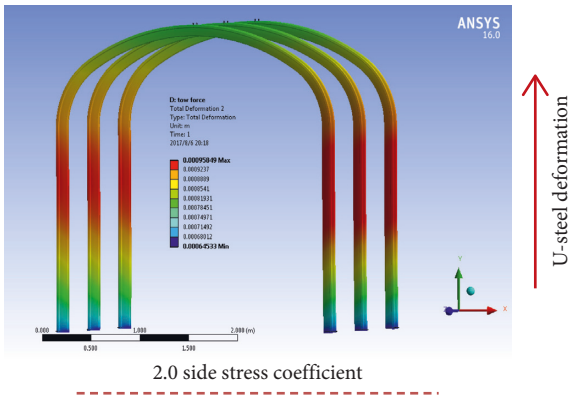

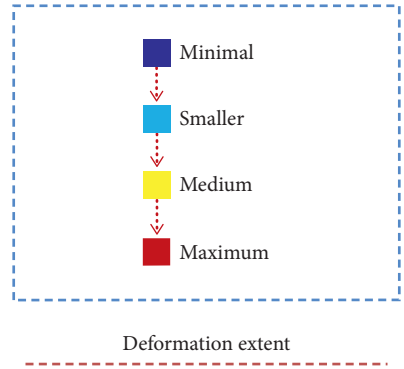

FIGURE 5: Deformation of the U-shaped steel with different lateral stress coefficients: (a) 0.8; (b) 1.0; (c) 1.2; (d) 1.5; (e) 2.0. Dark blue to deep red, small to large deformation. The maximum values were 1.3533 mm, 1.2614 mm, 1.1701 mm, 1.0344 mm, and 0.95849 mm, respectively.

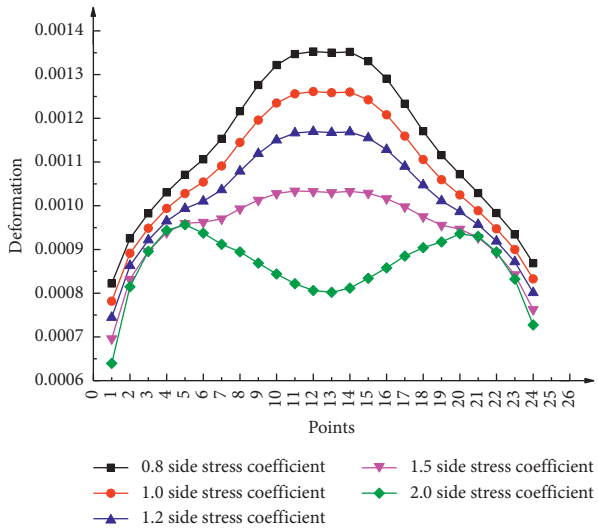

FIGURE 6: The deformation of various side stress coefficients. The black broken line, red broken line, blue broken line, pink broken line, and green line represent the deformation of 0.8, 1.0, 1.2, 1.5, and 2 side stress coefficients, respectively.

From the maximum deformation shown in Figure 9, it is known that the U-shaped steel bearing capacity is mainly on the top, and with the increase in the contact area, the maximum deformation is decreasing.

Data extracted for analysis are shown in Figure 10. Figure 10(a) shows oscillating discontinuity at monitoring points numbered 8 to 17 (U-shaped steel roof beam). According to the lateral stress coefficient influence factors, vertical stress plays a leading role when the lateral stress coefficient is 1.0. Therefore, the deformation part is the top beam part, and at this time, the value of the top beam part is an oscillating discontinuity, which indicates that the local stress concentration forms when the contact area is small. As shown in Figures 10(b)–10(f), with the increase in the contact area ratio, the U-shaped steel contact with the surrounding rock is increased. The concentration stress of the untouched part of the U-shaped steel roof beam is transferred to other contact parts, and the concentration stress is released eliminating the oscillating discontinuity phenomenon.

To compare the deformation of different contact area ratios, the data of each monitoring point at 1.5 m spacing are drawn in Figure 11. Among them, under the condition of complete contact, the deformation of each monitoring point is smaller than other conditions, which indicates that the coupling effect of U-shaped steel and surrounding rock is good, the overall force is enhanced, and the supporting effect is better. When the contact area ratio is 1/4, there is a significant jump at monitoring points 8 to 17, that is, the stress concentration part. That is to say, for a part of U-shaped steel, the pressure increases when the force area decreases, and the maximum stress value in the local region of the member is higher than the average stress value.

3.4. Force Analysis of U-Shaped Steel under Dynamic Disturbance. With the increase in depth, underground stress activity intensifies, which often has a great influence on tunnel stability [28]. Therefore, based on the original model, a dynamic disturbance was added to simulate its effect on the supporting body, as shown in Figure 12. Based on this analysis under two schemes, first, the dynamic block sustained 0.1 s impact on the rock mass at the velocity of 60 m/s. Second, the dynamic block sustained 0.15 s impact on the rock mass at the velocity of 50 m/s. The impulse of scheme 1 is less than that of scheme 2, which indicates that the acting force of scheme 1 is less than that of scheme 2.

The following results were obtained by simulation of the two schemes, as shown in Figure 13. From Figure 13(c), it is concluded that the deformation of the left beam is clearly close to the dynamic disturbance, especially at the bottom. From Figure 13(f), it is concluded that the maximum deformation occurs at the 45° oblique beam, while the lateral beam and the bottom are relatively small. Figure 13(d) is more uniform than Figure 13(a), and there is no irregular deformation distribution in the model. In Figure 13(f),

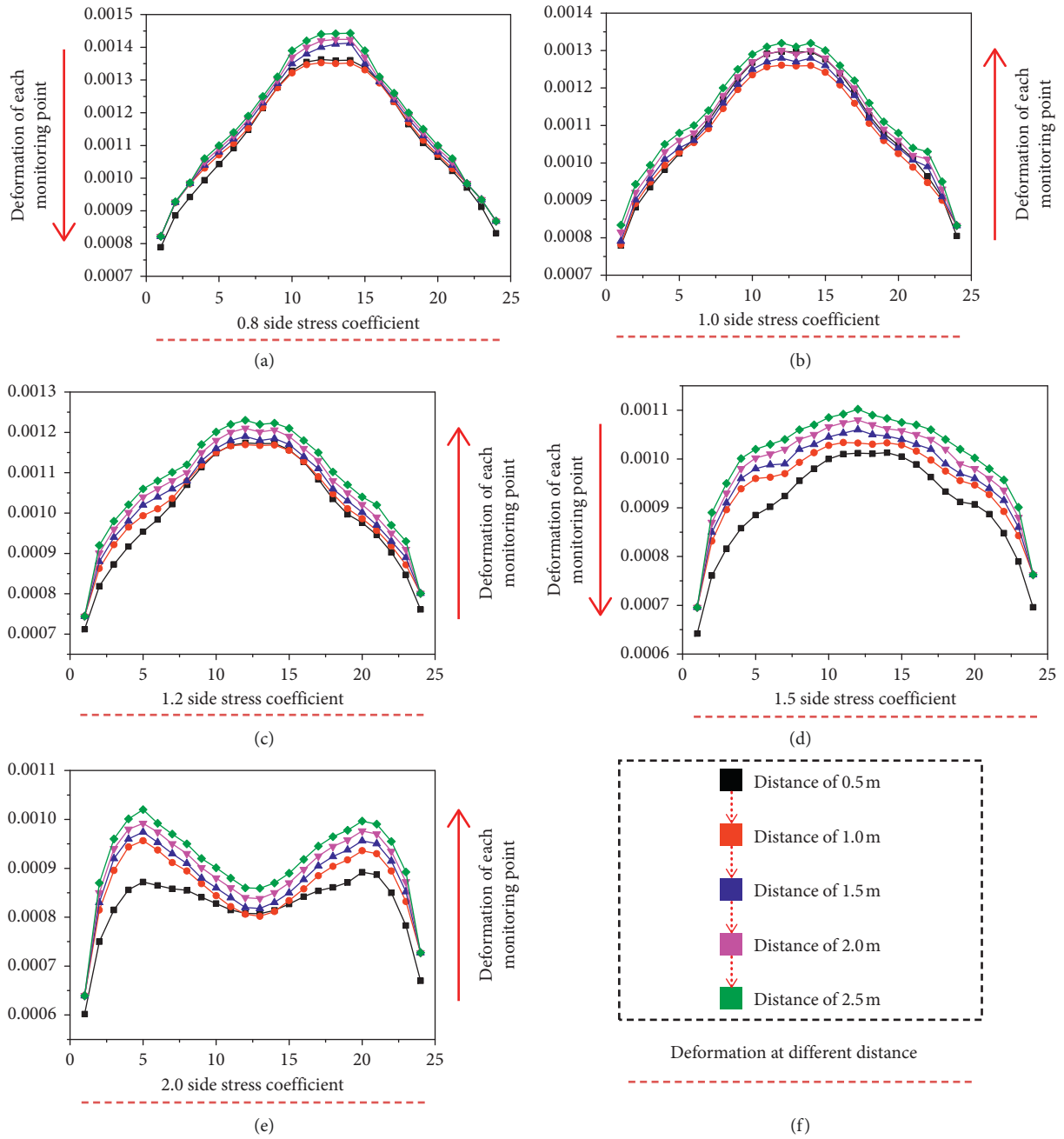

Figure 7: The deformation of various monitoring points with different factors. (a) Deformation of the 0.8 side stress coefficient; (b) deformation of the 1.0 side stress coefficient; (c) deformation of the 1.2 side stress coefficient; (d) deformation of the 1.5 side stress coefficient; (e) deformation of the 2.0 side stress coefficient. The black curve represents the distance of 0.5 m; the red curve, the distance of 1.0 m; the blue curve, the distance of 1.5 m; the pink curve, the distance of 2.0 m; the green curve, the distance of 2.5 m.

relative to Figure 13(c), the deformed section of the monitoring point is transferred from the lateral beam to the inclined 45° beam. This shows that, with the increase in dynamic disturbance time, the main force points of U-shaped steel will change and transfer to the top beam.

In view of this, the deformation and equivalent stress values of the two schemes are extracted for analysis, as shown in Figure 14. It can be seen from Figure 14(a) that the deformation of the power block is larger if the force is large. The equivalent stress of the supporting body is larger if the speed of the power block is larger at monitoring points 1 to 7, as shown in Figure 14(b). However, monitoring points 8 to 24 do not follow this rule. It is thus evident that the velocity affects the supporting body, and the magnitude of the equivalent effective stress depends on the distance between the power block and the supporting body.

Metal mine tunnels are usually carried out by blasting. The existence of shock waves caused by blasting affects the

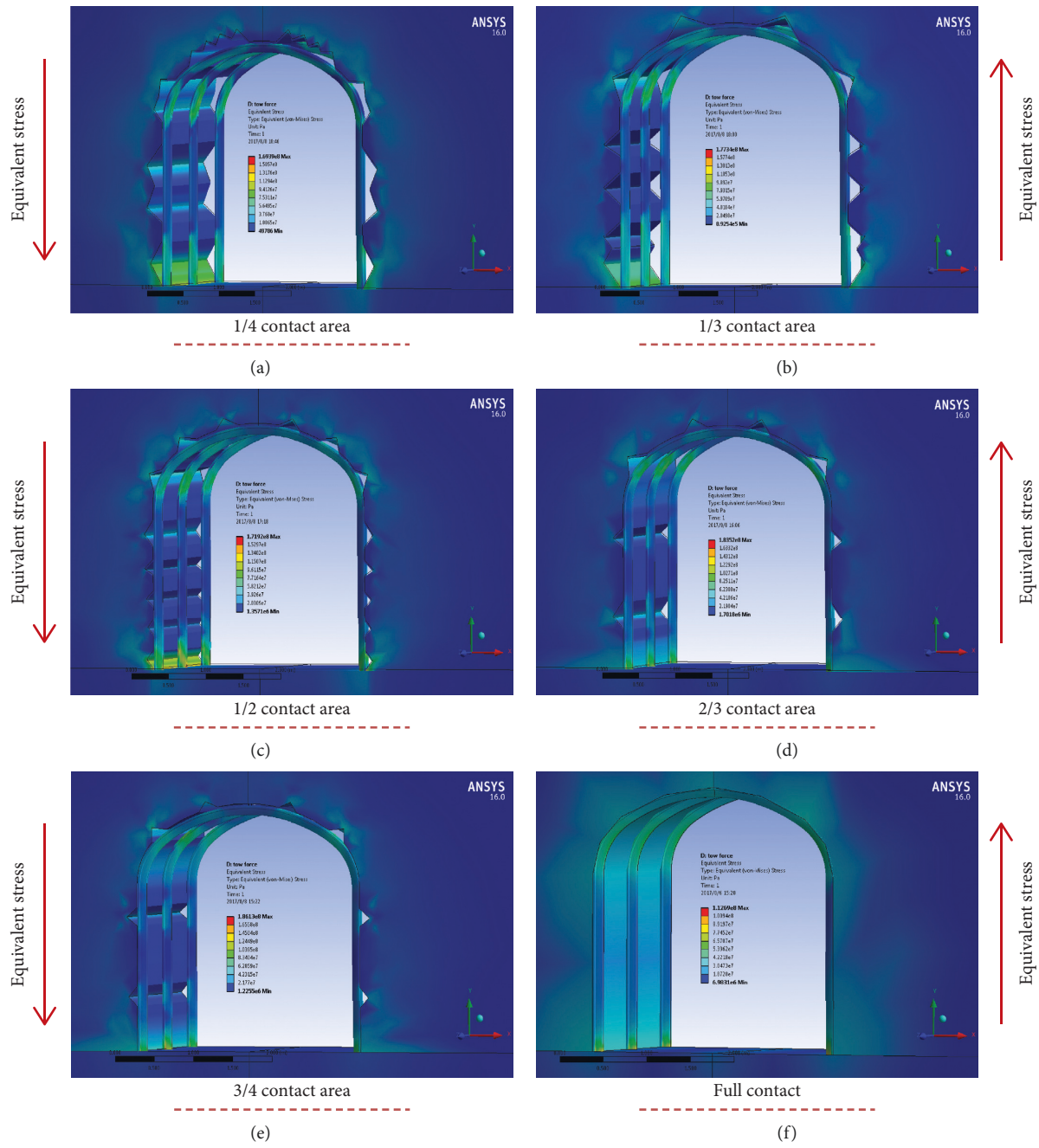

Figure 8: The overall equivalent stress. The equivalent stress is based on the stress contour line to express the stress distribution in the model. It can clearly describe the variation in a result in the whole model so that it can quickly determine the most dangerous region in the model. The equivalent stress maps with contact area ratios of (a) 1/4, (b) 1/3, (c) 1/2, (d) 2/3, (e) 3/4, and (f) 1 are shown. The maximum values were 1.6939*e*8 Pa, 1.7734*e*8 Pa, 1.7192*e*8 Pa, 1.8352*e*8 Pa, 1.8613*e*8 Pa, and 1.1269*e*8 Pa, respectively.

safety of underground mining. Therefore, the influence of blasting disturbance on U-shaped steel during tunnel excavation is simulated, as shown in Figure 15. Subsequently, according to different explosive quantities, the blasting is carried out in the adjacent tunnel, and the result is shown in Figure 16. To further study the supporting mechanism of U-shaped steel, the blasting wave is extracted and analyzed, as shown in Figure 17. It can be seen from Figures 17(a)–17(d) that the positive and negative signs of velocity represent directionality, and the maximum vibration velocity approximately increases with the increase in explosive content.

Finally, the stress values of U-shaped steel are extracted, as shown in Figure 18. With the increase in explosive quantity, the equivalent stress decreases first and then increases. The possibility of this phenomenon is twofold: first, the effect of energy transfer in the rock mass is different when the vibration frequency of different

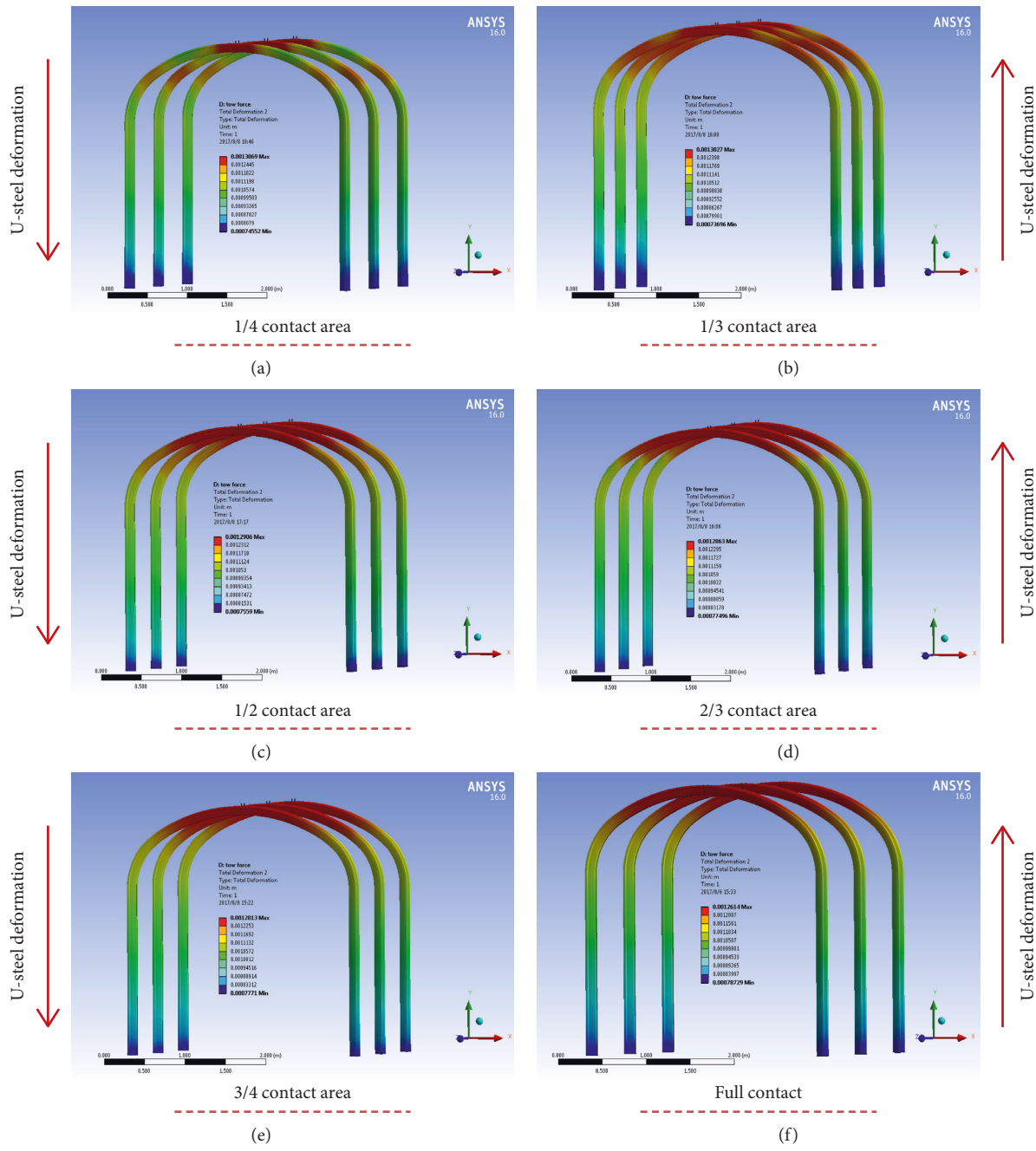

Figure 9: Total deformation of U-shaped steel with the contact area ratios of (a) 1/4, (b) 1/3, (c) 1/2, (d) 2/3, (e) 3/4, and (f) 1/1. The maximum deformation values were 1.3069 mm, 1.3027 mm, 1.2906 mm, 1.2863 mm, 1.2813 mm, and 1.2614 mm, respectively.

explosions is different. Second, the blast wave propagates in the air and rock mass to produce reflection. It is possible that the blast wave and reflected wave are offset, and it is also possible to stack.

In view of this, it is not ideal to consider only the equivalent stress, so the strain value of the corresponding model is extracted, as shown in Figure 19. The strain value is positive, indicating that the stress of U-shaped steel is tensile stress, and vice versa for compressive stress. It can be seen that the main force of U-shaped steel in Model 1 and Model 3 is tensile stress. Model 2 and Model 4 are mainly under compressive stress. Therefore, the force of U-shaped steel changed from tensile to compressive due to the change in explosive content, showing that it is within the disturbance range (no more than tensile-compressive strength), and the support's physical strength can effectively guarantee the safety of the supporting section. It can be seen from Figures 17 and 18 that the explosion wave propagation will produce reflected waves in the rock mass. Based on the different blasting frequency, the vibration wave will be superimposed or offset; the smaller the blasting vibration frequency is, the greater the impact of the supporting body is.

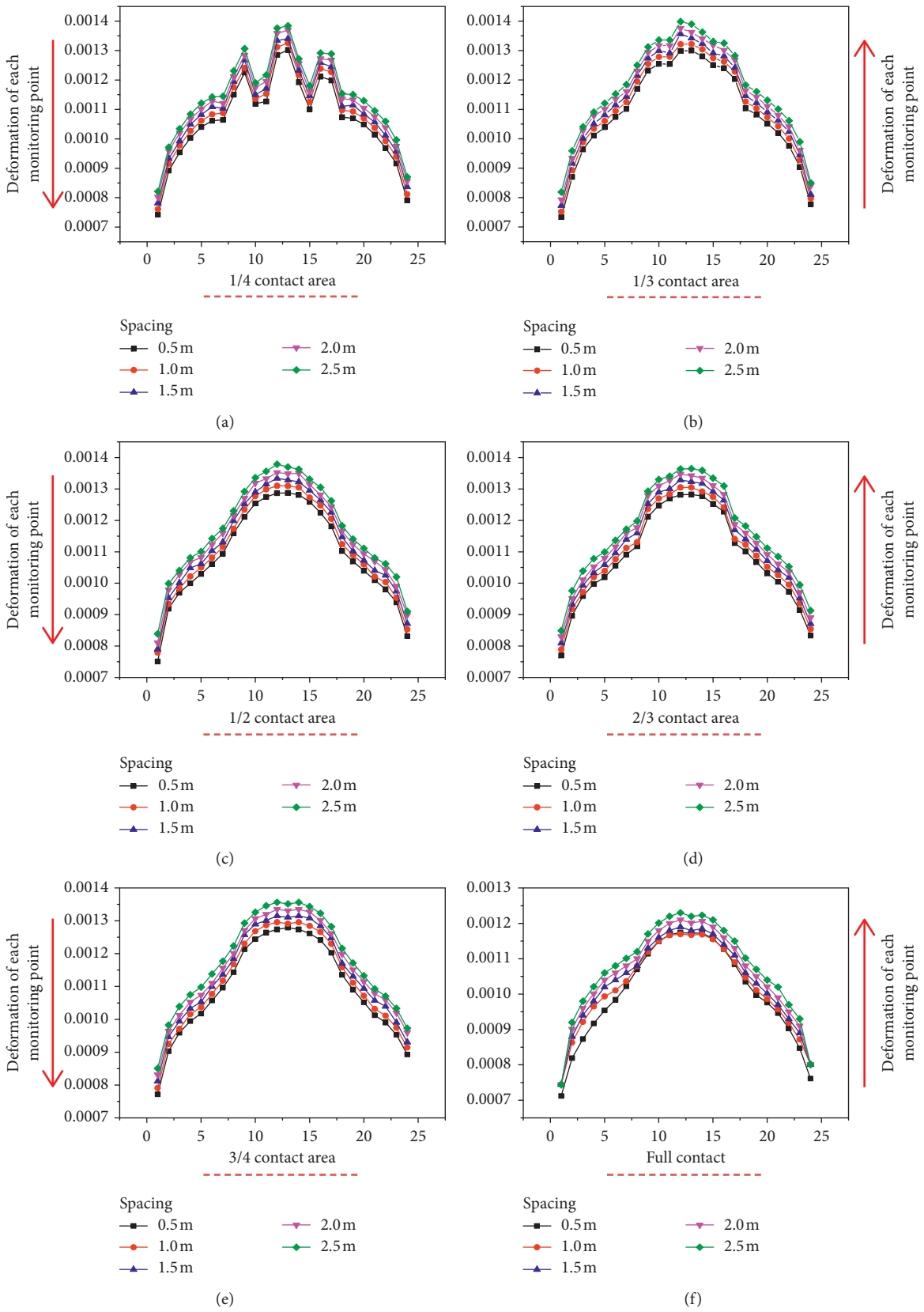

Figure 10: Various factors and contact area ratio for the deformation: (a) 1/4; (b) 1/3; (c) 1/2; (d) 2/3; (e) 3/4; (f) 1/1. The black curve represents the distance of 0.5 m; the red curve, the distance of 1.0 m; the blue curve, the distance of 1.5 m; the pink curve, the distance of 2.0 m; the green curve, the distance of 2.5 m.

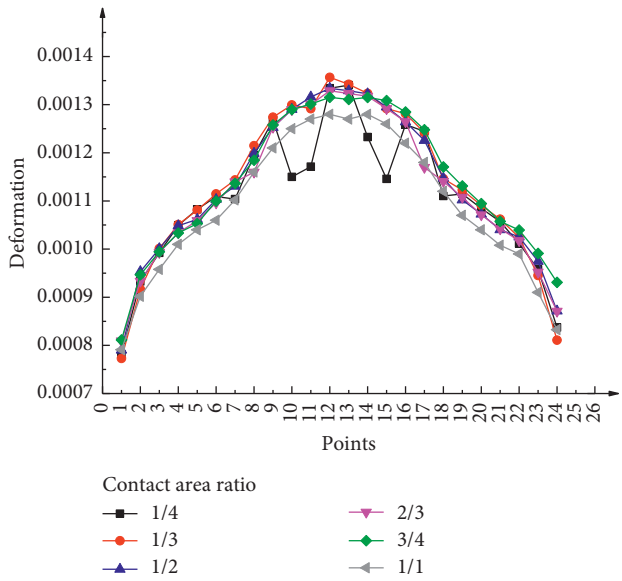

Figure 11: The deformation of various contact area ratios. The black curve represents the ratio of contact area of 1/4, the red curve represents the ratio of contact area of 1/3, the blue curve represents the ratio of contact area of 1/2, the pink curve represents the ratio of contact area of 2/3, the green curve represents the ratio of contact area of 3/4, and the gray curve represents complete contact.

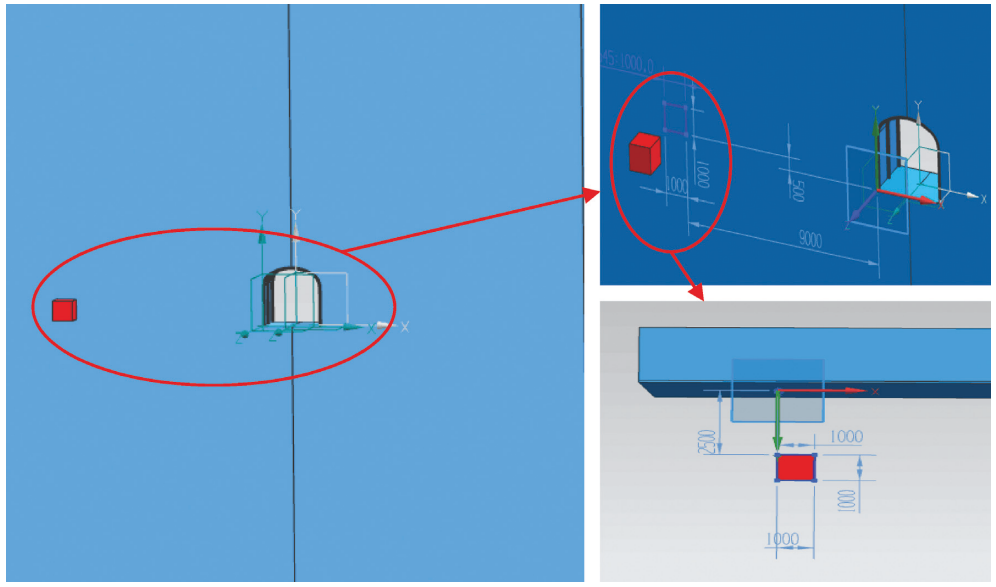

Figure 12: Dynamic impact model diagram. The blue model represents the rock mass, the black one represents the U-shaped steel, the red square represents the dynamic impact block, and the dynamic impact block from the laneway is $(x: -9.0, y: 0.5, z: 2.5)$.

4. Field Tests and Discussion

The data and results obtained from the above numerical simulation were compared and analyzed according to the actual situations. Figure 20 is a plane diagram of −630 m middle section of Jiaojia Gold Mine, Shandong Gold Group, China. The U-shaped steel of the ramp road was selected for analysis, as shown in Figure 21.

Combined with the rock mass characteristic parameters in the support section, the numerical simulation test was carried out with the formula derived in this paper and the field blasting data, and the results were analyzed, as shown in Figure 22. The simulated blasting wave data generated by 40 kg explosives were compared with the spot blasting data. The actual blasting velocity waveform basically coincided with the simulated blasting waveform, the actual waveform was slightly larger, and the error between the two waveforms was approximately 10%. Then, the field data are added to the U-shaped steel surrounding rock coupling formula to verify the calculation results shown in Table 1. Apparently,

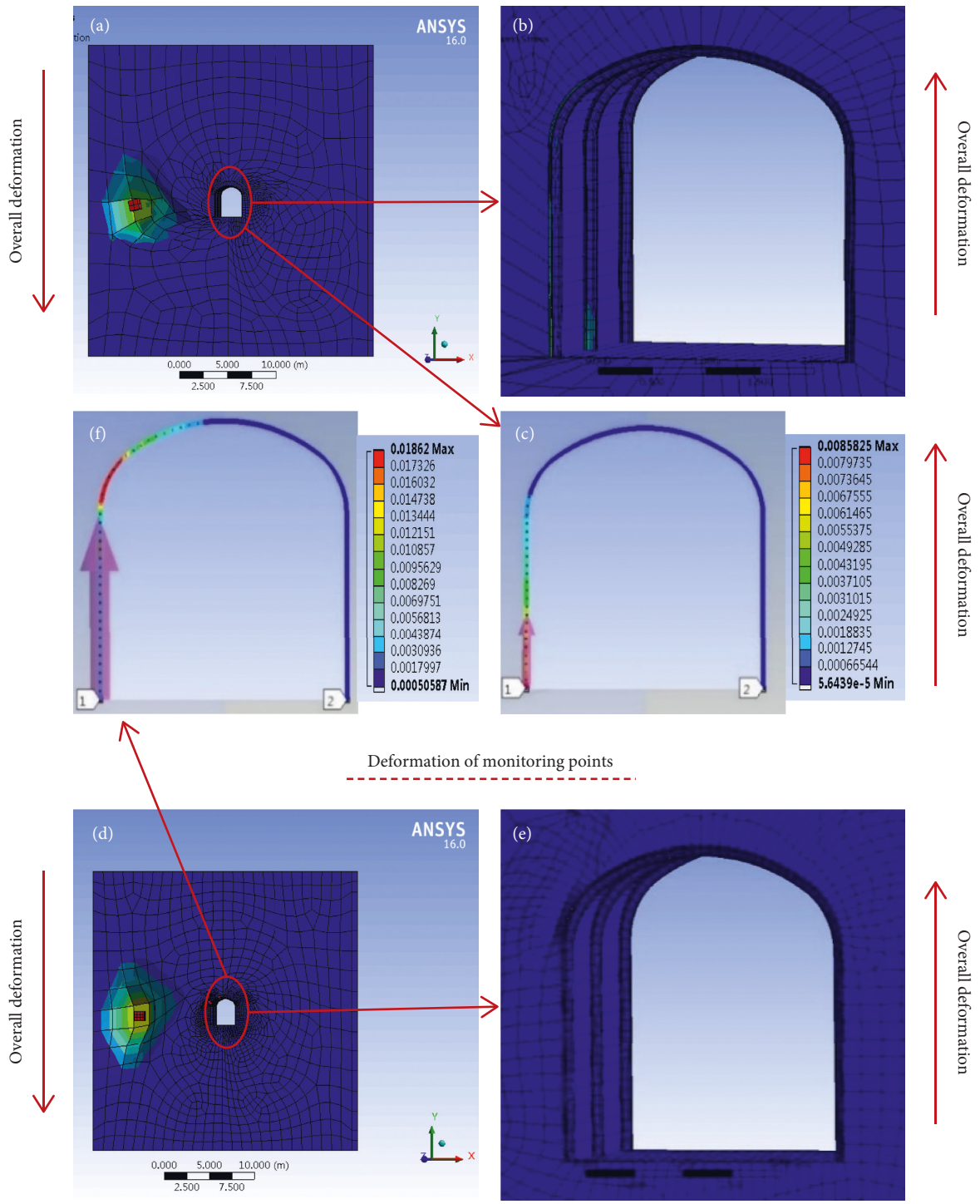

Figure 13: Overall disturbance distortion. (a, d) Total deformation. (b, e) U-shaped steel magnification diagram. (b, e) Deformation of U-shaped steel monitoring point. (a), (b), and (c) are the numerical simulation of scheme 1, and (d), (e), and (f) are the numerical simulation of scheme 2.

excluding the impact of groundwater and rock joints and fractures, the U-shaped steel spacing is 1.5 m, which meets the stability requirements.

Many scholars have studied the stress concentration of rocks [29–32]. Considering the loosening of underground rocks, the existence of joints, and so on, the vertical stress was calculated according to the actual mine conditions and the tunnel depth. Then, the vertical stress changes under different stress concentration factors were calculated according to the fitting condition of the surrounding rock and steel support, as shown in Figure 23. It can be seen that higher stress concentration factors cause a worse degree of fit between the surrounding rock and the steel support and the greater vertical stress on the steel support. The stent will

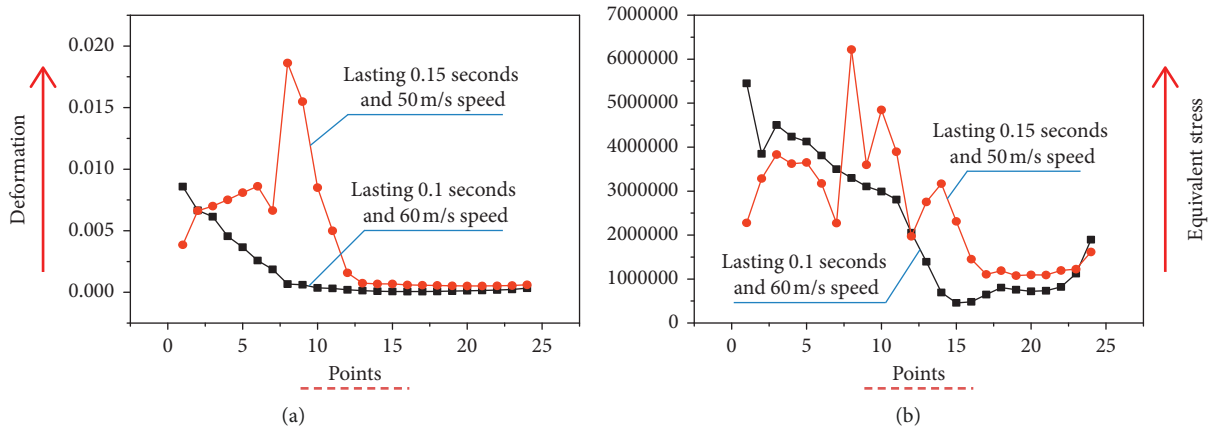

Figure 14: Deformation (a) and equivalent stress (b) of the monitoring points. Black curve stands for scheme 1, and red curve represents scheme 2.

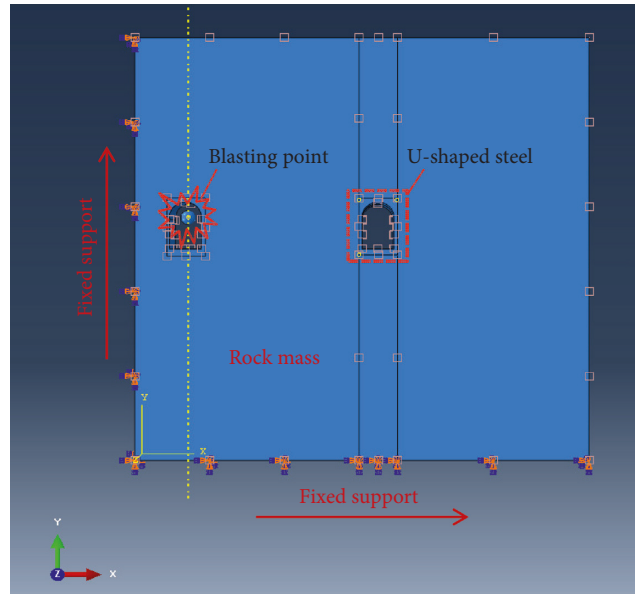

Figure 15: Blasting disturbance model. The red dashed line partly represents the U-shaped steel supporting tunnel, 9 m from the explosion point. The blue represents the rock mass, and the model boundary is fixed.

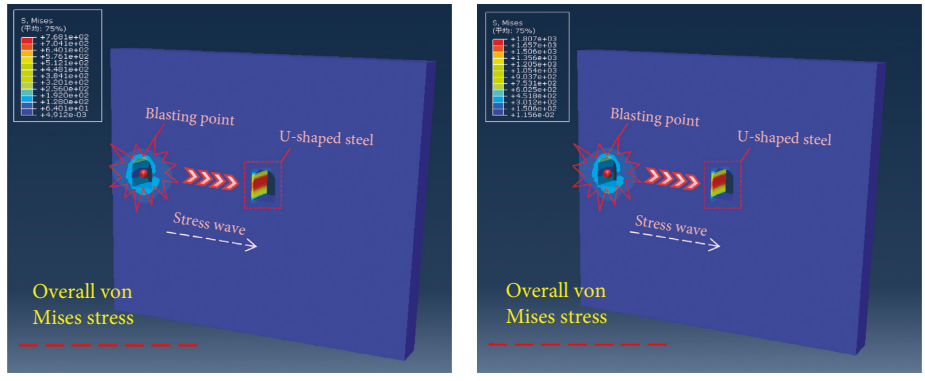

Figure 16: Continued.

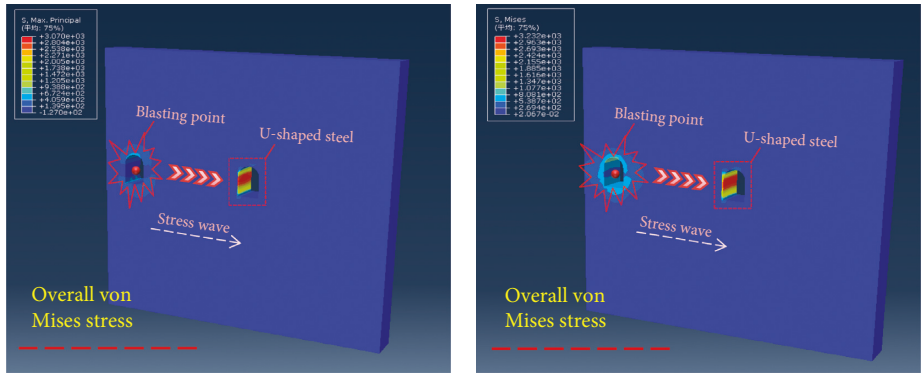

(c) (d)

Figure 16: The overall equivalent stress for blasting. The effect of blasting disturbance on U-shaped steel is obtained under the explosive charge of 32 kg (a), 40 kg (b), 48 kg (c), and 60 kg (d). Explosives act on U-shaped steel in the form of explosive waves through rock mass. The maximum equivalent stress is 7.6812 Pa, 1.8073 Pa, 3.073 Pa, and 3.2323 Pa, respectively. Therefore, the damage caused by the explosive wave of 60 kg explosive amount to the U-shaped steel also does not reach the yield strength.

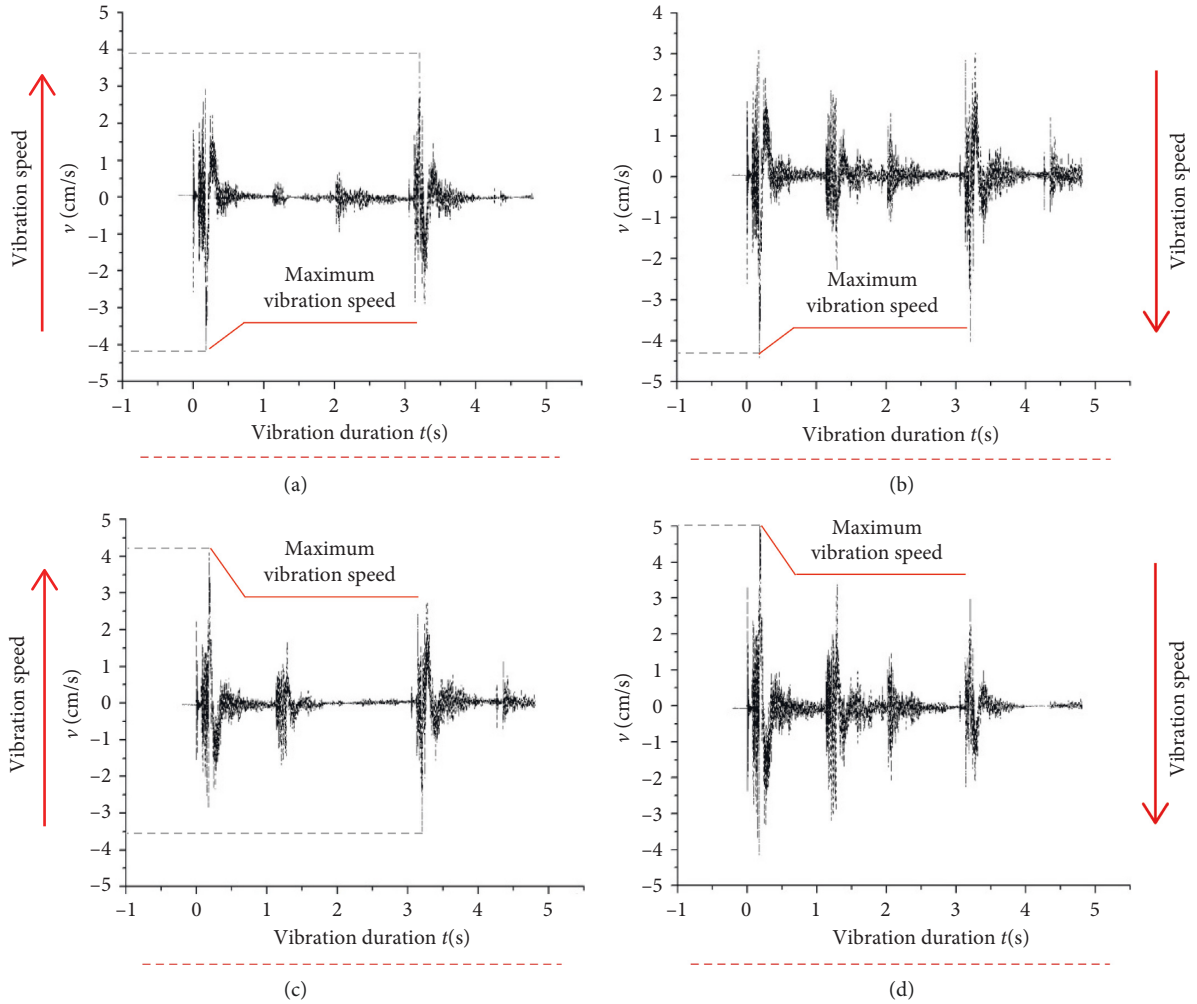

Figure 17: Burst disturbance waveform. The velocity waveforms produced by blasting of 32 kg, 40 kg, 48 kg, and 60 kg explosives are represented, and the main frequency is 74 Hz, 3.7 Hz, 96 Hz, and 4.5 Hz, respectively. (a) Explosive content 32 kg and main vibration frequency 74 Hz. (b) Explosive content 40 kg and main vibration frequency 3.7 Hz. (c) Explosive content 48 kg and main vibration frequency 96 Hz. (d) Explosive content 60 kg and main vibration frequency 4.5 Hz.

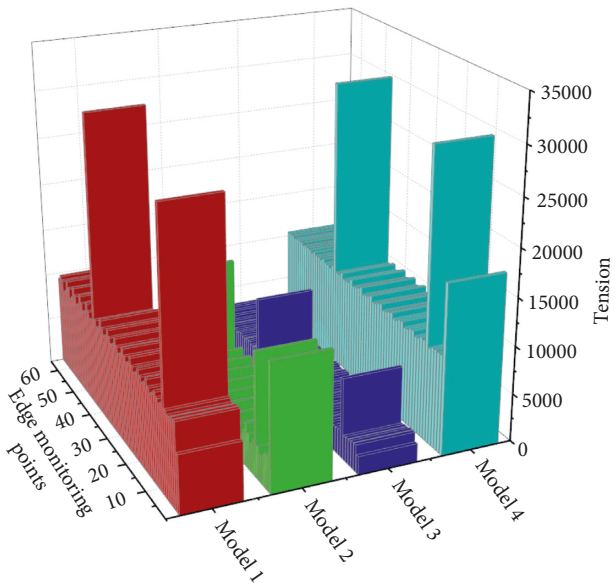

Figure 18: Equivalent stress histogram of U-shaped steel under blasting disturbance. Model 1 to Model 4 refer to the equivalent stresses of U-shaped steels with explosion amounts of 32 kg, 40 kg, 48 kg, and 60 kg, respectively.

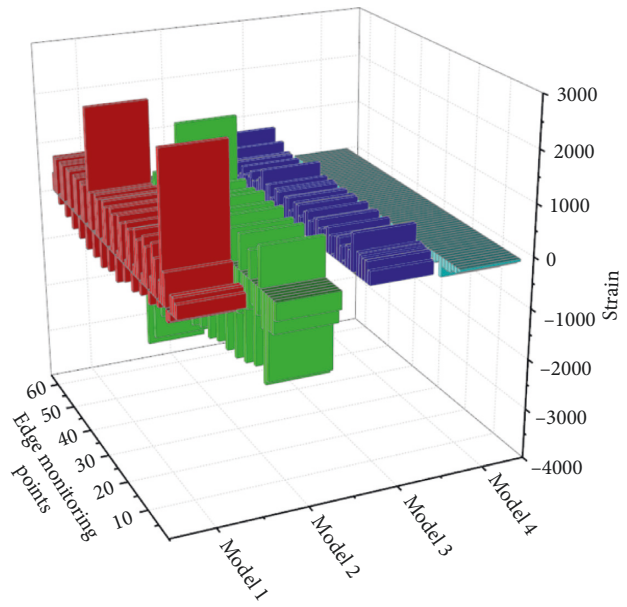

Figure 19: Strain histogram of U-shaped steel under blasting disturbance. Model 1 to Model 4 refer to the strain of U-shaped steels with explosion amounts of 32 kg, 40 kg, 48 kg, and 60 kg, respectively.

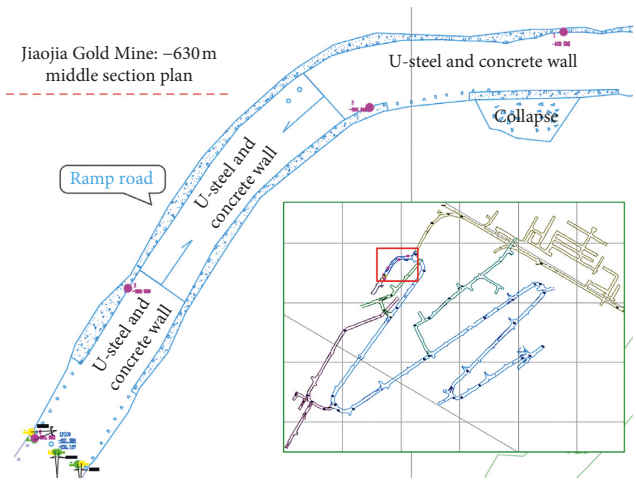

Figure 20: Jiaojia Gold Mine: −630 m midsection plan.

damage, and there is loss of support capacity when the vertical stress is greater than the yield stress of the steel support.

To obtain reasonable steel support spacing, the vertical stress of steel support under different stress concentration factors was considered. The processed data were plotted in Figure 24. When the support stress exceeds the yield strength of the material, the steel frame will be destroyed and the support strength will be lost. Moreover, the higher the stress concentration factor, the greater the vertical stress on the U-shaped steel support. When the stress concentration factor is 12, the steel bracket spacing should be approximately 0.8 m to ensure the vertical stress is less than the yield strength. When the stress concentration factor is 9, the steel bracket spacing should be approximately 1.2 m to ensure the vertical stress is less than the yield strength. When the stress concentration factor is 6, the steel bracket spacing should be approximately 1.8 m to ensure the vertical stress is less than the yield strength. When the stress concentration factor is less than 6, the yield strength of the steel support is greater than the vertical stress of the support, and the steel support can play a good role to ensure that the surrounding rock of the tunnel is in a stable state. In practice, the stress concentration factor of U-shaped steel is generally between 6 and 9, and the spacing of 1.5 m can meet the safety requirements.

In this paper, the numerical simulation of steel support spacing, contact area, and lateral stress coefficient is taken

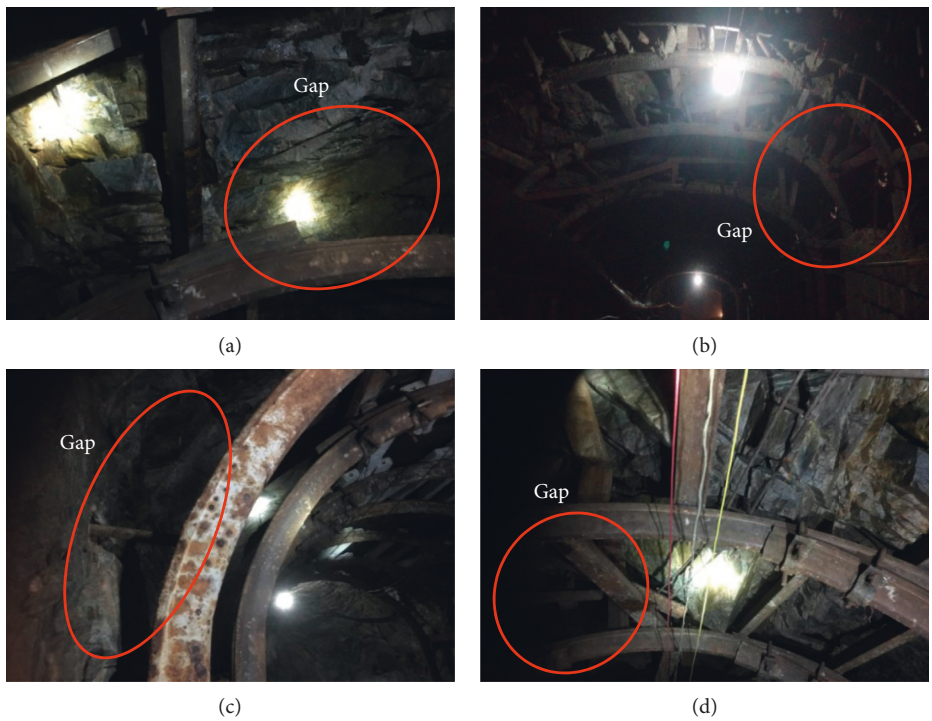

Figure 21: The −630 m middle ramp. The red circle in the diagram shows the degree of adhesion between U-shaped steel and surrounding rock. The average spacing of U-shaped steel is 1.5 m, and the contact area ratio is approximately 1/4.

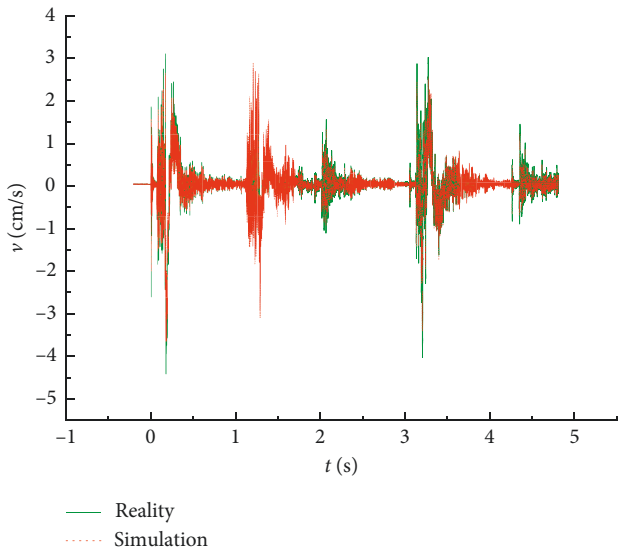

Figure 22: Real blasting wave (green wave) and simulated blasting wave (red dotted line wave).

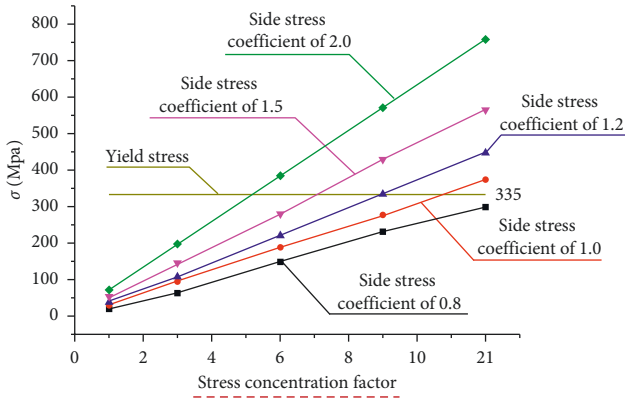

Figure 23: Vertical stress changes with different stress concentration factors. The black curve represents the equivalent stress of U-shaped steel with 0.8 side stress coefficient, the red curve represents the case of side stress coefficient 1.0, the blue curve represents the case where the side stress coefficient is 1.2, the pink curve represents the lateral stress coefficient of 1.5, the green curve represents the lateral stress coefficient of 2.0, and the brown represents the yield stress of U-shaped steel.

into account. Combined with blasting vibration, the optimized parameters of U-shaped steel are obtained. Furthermore, a coupled formula for the U-shaped steel and surrounding rock in deep three-center arch tunnels is put forward, and its correctness is verified.

5. Conclusions

U-shaped steel supports play an extremely important role in deeply buried tunnels under dynamic disturbance. We apply the coupling formula and stress concentration factor of U-shaped surrounding rock to study tunnel stability. The correctness of the formula is verified by using surrounding rock data and numerical simulation. Factors such as disturbance angular frequency, velocity, and time are selected as safety factor indexes of U-shaped steel.

Through the numerical simulation of different spacings, side stress coefficients, contact area ratios, and explosive quantities, the following conclusions can be drawn: (i) the

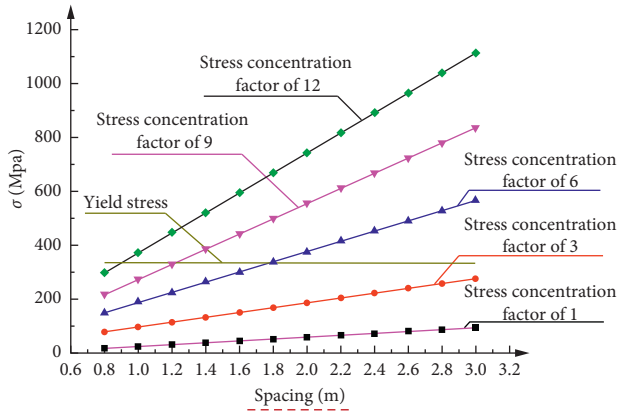

Figure 24: Vertical stress variation under different stress concentration factors at different spacings. The black curve represents the equivalent stress of U-shaped steel under the concentration stress coefficient of 1, the red curve represents the case where the concentration stress coefficient is 3, the blue curve represents the case where the concentration stress coefficient is 6, the pink curve represents the concentration stress coefficient of 9, the green curve represents the concentration stress coefficient of 12, and the brown represents the yield stress of U-shaped steel.

outburst deformation section of U-shaped steel with lateral stress coefficient less than 1 is the part of the top beam. With the increase in lateral stress coefficient, the overall deformation shows a downward trend, indicating that the lateral stress is the dominant force in deep ground stress activity. (ii) When the contact area is small, a stress concentration will form, which is one of the factors leading to the instability of U-shaped steel. (iii) The stability of U-shaped steel is tested by simulating dynamic impact and blasting vibration. The results clearly show that the U-shaped steel with a spacing of 1.5 m can meet the support requirements of grade V surrounding rock.

Data Availability

The data used to support the findings of this study are available from the corresponding author upon request.

Conflicts of Interest

The authors declare that they have no conflicts of interest.

Acknowledgments

This study was supported by the National Natural Science Foundation of China (51574093 and 51774101), the High Level Innovative Talents Training Project in Guizhou Province (Project no. 2016-4011), the Major Application Foundation Research Project of Guizhou Province (JZ2014-2005), the Guizhou University Talent Introduction Foundation (Project no. 2017-63), the First-Class Discipline Construction Project of Civil Engineering in Guizhou Province (Project no. QYNYL[2017]0013), the Cultivation Project of Guizhou University (Project no. [2017]5788-49), and the Guizhou Mining Power Disaster Early Warning and Control Technology Innovation Team Fund.

References

[1] Compiling Committee of China, *China Coal Industry Yearbook*, China Coal Industry Press, Beijing, China, 2009.

[2] L. J. Dong, W. W. Shu, X. B. Li, G. J. Han, and W. Zou, "Three dimensional comprehensive analytical solutions for locating sources of sensor networks in unknown velocity mining system," *IEEE Access*, vol. 5, no. 99, pp. 11337–11351, 2017.

[3] L. J. Dong, D. Y. Sun, X. B. Li, and K. Du, "Theoretical and experimental studies of localization methodology for AE and microseismic sources without pre-measured wave velocity in mines," *IEEE Access*, vol. 5, pp. 16818–16828, 2017.

[4] L. J. Dong, J. Wesseloo, Y. Potvin, and X. B. Li, "Discrimination of mine seismic events and blasts using the Fisher classifier, naive bayesian classifier and logistic regression," *Rock Mechanics and Rock Engineering*, vol. 49, no. 1, pp. 183–211, 2015.

[5] L. J. Dong, J. Wesseloo, Y. Potvin, and X. B. Li, "Discriminant models of blasts and seismic events in mine seismology," *International Journal of Rock Mechanics and Mining Sciences*, vol. 86, pp. 282–291, 2016.

[6] L. J. Dong, D. Y. Sun, X. B. Li, and Z. L. Zhou, "Interval nonprobabilistic reliability of a surrounding jointed rockmass in underground engineering: a case study," *IEEE Access*, vol. 5, pp. 18804–18817, 2017.

[7] L. J. Dong, D. Y. Sun, X. B. Li et al., "Interval nonprobabilistic reliability of surrounding jointed rockmass considering microseismic loads in mining tunnels," *Tunnelling and Underground Space Technology*, vol. 81, pp. 326–335, 2018.

[8] X. B. Li, Z. L. Zhou, Z. Y. Ye et al., "Study of rock mechanical characteristics under coupled static and dynamic loads," *Chinese Journal of Rock Mechanics and Engineering*, vol. 27, no. 7, pp. 1387–1395, 2008.

[9] X. B. Li, Y. J. Zuo, and C. D. Ma, "Constitutive model of rock under coupled static-dynamic loading with intermediate strain rate," *Chinese Journal of Rock Mechanics and Engineering*, vol. 25, no. 5, pp. 865–874, 2006.

[10] X. B. Li, F. Feng, and D. Y. Li, "Numerical simulation of rock failure under static and dynamic loading by splitting test of circular ring," *Engineering Fracture Mechanics*, vol. 188, no. 1, pp. 184–201, 2017.

[11] X. B. Li, F. Q. Gong, M. Tao et al., "Failure mechanism and coupled static-dynamic loading theory in deep hard rock mining: a review," *Journal of Rock Mechanics and Geotechnical Engineering*, vol. 9, no. 4, pp. 767–782, 2017.

[12] A. Kirsch, "Experimental investigation of the face stability of shallow tunnels in sand," *Acta Geotechnica*, vol. 5, no. 1, pp. 43–62, 2010.

[13] S. Q. Yang, M. Chen, H. W. Jing, K. F. Chen, and B. Meng, "A case study on large deformation failure mechanism of deep soft rock roadway in Xin'An coal mine, China," *Engineering Geology*, vol. 217, pp. 89–101, 2017.

[14] Y. C. Wang, H. W. Jing, H. J. Su, and J. Y. Xie, "Effect of a fault fracture zone on the stability of tunnel-surrounding rock," *International Journal of Geomechanics*, vol. 17, no. 6, article 04016135, 2016.

[15] L. Malmgren, E. Nordlund, and S. Rolund, "Adhesion strength and shrinkage of shotcrete," *Tunnelling and Underground Space Technology*, vol. 20, no. 1, pp. 33–48, 2005.

[16] L. Malmgren and E. Nordlund, "Interaction of shotcrete with rock and rock bolts-A numerical study," *International Journal of Rock Mechanics and Mining Sciences*, vol. 45, no. 4, pp. 538–553, 2008.

[17] R. B. Dharma and K. H. Tan, "Rotational capacity of steel I-beams under fire conditions Part II: numerical simulations," *Engineering Structures*, vol. 29, no. 9, pp. 2403–2418, 2007.

[18] W. B. Zhou, S. J. Li, Z. Huang, and L. Z. Jiang, "Distortional buckling of I-steel concrete composite beams in negative moment area," *Steel and Composite Structures*, vol. 20, no. 1, pp. 57–70, 2016.

[19] R. H. Cao, P. Cao, and H. Lin, "Support technology of deep roadway under high stress and its application," *International Journal of Mining Science and Technology*, vol. 26, no. 5, pp. 787–793, 2016.

[20] J. A. Hudson and J. P. Harrison, *Engineering Rock Mechanics: An Introduction to the Principles*, X. T. Feng, Ed., pp. 220–234, Science Press, Beijing, China, 2009.

[21] H. P. Kang, J. H. Wang, and J. Lin, "Reinforcement technique and its application in complicated tunnels in underground coal mines," in *Proceeding of 12th ISRM International Congress on Rock Mechanics Harmonising Rock Engineering and the Environment*, pp. 1527–1532, Beijing, China, October 2011.

[22] J. Z. Liu, N. Zhang, X. G. Zheng, and B. G. Wang, "Research on buckling failure mechanism of U type steel support loaded deviating longitudinally," *Journal of China Coal Society*, vol. 36, no. 10, pp. 1647–1652, 2011.

[23] Y. Y. Jiao, L. Song, X. Z. Wang, and A. Coffi Adoko, "Improvement of the U-shaped steel sets for supporting the roadways in loose thick coal seam," *International Journal of Rock Mechanics and Mining Sciences*, vol. 60, no. 2, pp. 19–25, 2013.

[24] G. Y. Hou, "Review of interaction mechanism between surrounding rock and support and analysis of conceptual model of rheological deformation mechanism," *Chinese Journal of Rock Mechanics & Engineering*, vol. 27, no. 2, pp. 3618–3629, 2008.

[25] Y. J. Zuo, S. C. Li, S. F. Qin, and L. P. Li, "A catastrophe model for floor water-resisting key stratum instability induced by dynamic disturbance," *Rock & Soil Mechanics*, vol. 31, no. 8, pp. 2361–2366, 2010.

[26] L. J. Dong and G. Y. Zhao, "Unascertained average classification method for classifying surrounding rocks of mining tunnels," *Journal of PLA University of Science & Technology*, vol. 10, no. 6, pp. 575–579, 2009.

[27] J. Dundurs and M. S. Lee, "Stress concentration at a sharp edge in contact problems," *Journal of Elasticity*, vol. 2, no. 2, pp. 109–112, 1972.

[28] V. N. Oparin, I. I. Ainbinder, Y. I. Rodionov et al., "Concept of a mine of tomorrow for deep mining at gentle copper-and-nickel deposits," *Journal of Mining Science*, vol. 43, no. 6, pp. 646–654, 2007.

[29] H. Norio and K. Yasuhiro, "Calculation of stress intensity factor from stress concentration factor," *Engineering Fracture Mechanics*, vol. 10, no. 2, pp. 215–221, 1978.

[30] G. Senfaute, M. A. Heib, J. P. Josien, and J. F. Noirel, "Detection and monitoring of high stress concentration zones induced by coal mining using numerical and microseismic method," in *Proceedings of 5th International Symposium on "Rockbursts and seismicity in mines"*, Sandton, South Africa, September 2001.

[31] M. Y. Fattah, K. T. Shlash, M. J. M. Al-Waily, L. D. Suits, and T. C. Sheahan, "Stress concentration ratio of model stone columns in soft clays," *Geotechnical Testing Journal*, vol. 34, no. 1, article 103060, 2010.

[32] X. Y. Liu, A. M. S. Ammar, H. Lin, and J. Ren, "The stress concentration ratio of stone columns under confined condition," in *Proceedings of International Conference on Transportation Engineering*, pp. 4247–4255, Chengdu, China, July 2009.